Comparison of kinetic theory evaporation models for liquid thin-films

Eskil Aursand[a,*], Tor Ytrehus[a]

[a] *Department of Energy and Process Engineering, Norwegian University of Science and Technology (NTNU), Kolbjørn Hejes v. 1B, Trondheim N-7491, Norway*

Abstract

We summarize the background and derivation of non-equilibrium evaporation models from kinetic theory, and demonstrate how they may be applied in the context of fluid mechanics and heat transfer problems. We find that the linearized Boltzmann-equation Moment Method is a good trade-off between complexity and accuracy for practical purposes, and that the use of non-equilibrium evaporation models in general has significant quantitative and qualitative impact on the results.

Keywords: Evaporation, Thin-film, Non-equilibrium, Kinetic theory, Moment method

1. Introduction

When dealing with fluid mechanics problems that involve heat transfer and a liquid–vapor interface, it is usually necessary to specify some relation between the state of the continuum fluids on either side of the interface and the resulting evaporation or condensation flux across it. For simplicity, such phase transitions are often treated as quasi-equilibrium processes. In practice this means that the interface temperature is assumed to be continuous and exactly equal to the fluid's saturation temperature, which allows simple energy conservation considerations to close the problem. However, in reality phase transitions occur under non-equilibrium conditions (Carey, 1992). This means, among other things, that the liquid interface is in some unknown superheated state above the saturation temperature. The introduction of this new variable necessitates some new closure beyond just energy conservation, and this is where evaporation models enter.

Evaporation model introduce additional considerations from outside the realm of the continuum and local equilibrium assumptions made in fluid mechanics. One such framework is kinetic theory, which is the focus of the present work. Specifically the purpose of this work is to compare the different levels of model complexity, show how they may be applied in fluid mechanics, and investigate when they are necessary in practice.

The endeavor to apply kinetic theory to evaporation and condensation problems was pioneered by Hertz (1882) and Knudsen (1915). Their focus was on evaporation into near vacuum, but many aspects of the phenomenon were captured at least qualitatively, and the concepts were useful building blocks for modeling the more general case. A next step came with Schrage (1953), who introduced the effect of molecular collisions in the Hertz-Knudsen model. However, the theory still remained incomplete mainly because it missed the full dynamic connection between the flow parameters at the interphase surface and those far downstream. This gap was filled in through many later contributions, mainly in the period from the late 1960s and up to the turn of the century by authors who solved the Boltzmann equation, or models thereof, for the so-called *Knudsen layer*. This is a kinetic boundary layer between the evaporating surface and the external continuum flow, of thickness on the molecular mean free path scale. The current status has been dealt with in reviews by Kogan (1992) and Ytrehus (1997), based on developments by for instance Anisimov (1968), Shankar and Marble (1971), Patton and Springer (1969), Pao (1971a,b), Kogan and Makashev (1971), Cipolla Jr et al. (1974), Ytrehus (1974), Ytrehus (1977) , Sone and Onishi (1978), Aoki and Cercignani (1983), Aoki et al. (1991), Kogan and Abramov (1991), Sone and Sugimoto (1993), Ytrehus and Østmo (1996), to mention some of the basic contributions. A more recent review of the matter is given by Frezzotti and Barbante (2017).

Most of the models for evaporation and condensation problems developed from the 1970s and onwards are based on the fundamental Boltzmann equation of kinetic gas theory. A main improvement compared to the Hertz–Knudsen and Schrage models, which only took mass conservation into account, is that conservation of momentum and energy is also included. Initially, linear models for weak phase transfer rates were derived by, for instance Patton and Springer (1969), Shankar and Marble (1971), and Pao (1971a,b). Then, non-linear treatments for strong flow rates were considered by Kogan and Makashev (1971), Sone and Onishi (1978), using the BGK-collision model for numerical solutions of the Boltzmann equation, and

*Corresponding author
Email address: eskil.aursand@ntnu.no (Eskil Aursand)

by Ytrehus (1977) using a moment method to obtain analytical solutions to the Boltzmann equation for Maxwell molecules. There is good internal agreement among the results of these approaches, as well as with experiments by Mager et al. (1989) and with Monte Carlo simulations by Sibold and Urbassek (1993).

It is clear that the efforts put into the microscopic description of evaporation and condensation in the kinetic-theory community is significant. Unfortunately, a lot of these results remain quite inaccessible to the heat-transfer and fluid-mechanics communities due to the context and formalism in which they are presented. The purpose of the present paper is to demonstrate how such models may be applied to a relatively conventional problem with heat transfer and evaporation. In particular, it is to show how the choice of evaporation model matters, both between different kinetic-theory based models and when compared to the typical quasi-equilibrium approximation.

The kinetic-theory evaporation models compared herein represent a gradual increase in complexity and accuracy, while staying within the realm of analytical models that may reasonably be coupled to a heat-transfer or fluid-mechanics framework. The latter point excludes some highly advanced methods such as ones involving numerical solving of the Boltzmann and BGK equations. The models chosen here are the classical Hertz-Knudsen (Hertz, 1882; Knudsen, 1915) and Schrage-Mills (Schrage, 1953; Mills, 1995) models, and the more advanced Boltzmann-equation based *moment method* by Ytrehus (1997), in both its linearized and fully nonlinear form.

The macroscopic heat-transfer case used to demonstrate the practical use and significance of these models is deliberately chosen to be quite simple. This is to make the demonstration of how to apply kinetic-theory evaporation models as clear as possible, and to avoid losing track of the important points in the complexity of the macroscopic case itself. The case chosen herein is the evaporation of a thin liquid film on a heated horizontal surface. Such cases have been studied previously by authors such as Burelbach et al. (1988), Oron et al. (1997) and Craster and Matar (2009), but without any extensive discussion on the choice of evaporation model.

This paper is presented in two distinct parts: The first part, Sec. 2, establishes the context and formalism in which the kinetic-theory evaporation models are derived. This includes introducing central concepts such as the microscopic *Knudsen layer* outside an evaporating liquid surface, the temperature-jump that exists across it, and the fundamental driving force of evaporation: a difference between the liquid's saturation pressure and the actual applied pressure. The section then goes on to summarize the derivation of evaporation models of increasing complexity, all of which eventually make a prediction for an evaporation mass flux as a function of the aforementioned pressure-based driving force. In this context, which is local to the liquid–vapor interface, the models may then be compared in a way that is independent of any macroscopic case they may be applied to.

The second part, Sec. 3, demonstrates how these evaporation models may be coupled to the macroscopic liquid-film evaporation case. In particular, it shows the significance of model choice, especially when compared to the common quasi-equilibrium approximation: the assumption that the temperature at the liquid–vapor interface is continuous and equal to the saturation temperature.

2. Evaporation models

2.1. Problem description

The general practical problem is the determination of macroscopic interface boundary conditions and mass flux for an evaporating liquid–vapor interface. While the interface is commonly treated as having zero thickness in fluid mechanics, between the liquid bulk and the vapor bulk there are in fact two microscopic layers (see Fig. 1):

- *Interface transition*: A very rapid transition from a liquid-like density to a gas-like density across the distance of a few molecular diameters. This transition is so rapid on the scale of Fig. 1 that it is simply drawn as an instantaneous change at $z = 0$, which we will from here on refer to as *the liquid surface*. During evaporation the temperature also changes very rapidly across the interface, and on the scale of the illustration this is shown as a discontinuous jump from T_l to T_0.
- *Knudsen layer*: A layer between the liquid surface and the vapor bulk. Here the gas is heavily influenced by the evaporating interface and is in a non-equilibrium state. Its thickness is denoted δ_Kn, and is of the order of a few molecular mean free path lengths (λ). The Knudsen layer also involves a change in temperature, shown as a relatively slow change from T_0 to T_∞ in the illustration.

The molecular mean free path referred to above is the average distance traveled by a molecule in the gas before colliding with another. For an equilibrium distribution of monatomic particles, kinetic theory finds that the mean free path is

$$\lambda = \frac{k_\mathrm{B} T}{\sqrt{2} p \pi d^2}, \tag{1}$$

where T is the temperature, p is the pressure, d is the effective particle diameter and k_B is the Boltzmann constant. For atoms or molecules with diameters in the range of 0.25–1 nm, Eq. (1) implies that the mean free path under normal conditions is in the range of

$$\lambda \sim 10\text{–}150\,\mathrm{nm}, \tag{2}$$

In the Knudsen layer, the gas is more appropriately described by the Boltzmann equation (Cercignani, 1988), not

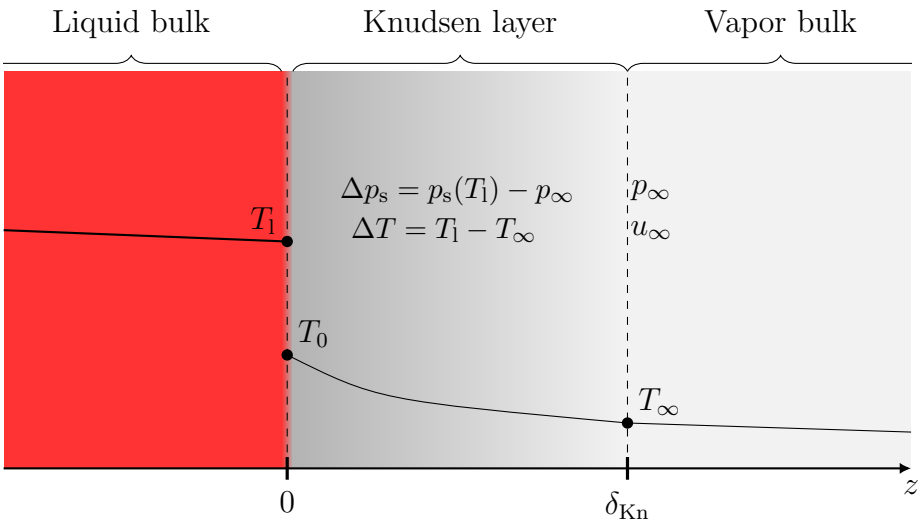

Figure 1: Illustration of an evaporating interface when zoomed in to the scale of the Knudsen layer. In this case, the heat driving the evaporation comes from the liquid bulk. The quantities at the outer edge of the Knudsen layer are typically labeled with ∞, because they are very far out on the scale of the molecular mean free path λ. The goal of the problem herein is to find the evaporation rate (here represented by u_∞) and total temperature difference (ΔT) that results from a driving force Δp_s.

the Navier–Stokes equation. The latter is in fact a special case simplification of the former for larger scales and close-to-equilibrium conditions (see Chapman–Enskog expansion (Kogan, 1992; Ytrehus, 1997)).

We wish to present evaporation models that are practically applicable to external macroscopic Navier–Stokes type problems. Even though the Knudsen layer is effectively invisible at these scales; if the problem involves evaporation the Knudsen layer has an effect by imposing boundary conditions at the seemingly zero-thickness liquid–vapor interface in the macroscopic problem. Specifically, the goal is to connect the following variables seen in Fig. 1:

- Input from macroscopic problem:
  - T_l: Temperature on liquid-side of the surface.
  - p_∞: Applied pressure from the vapor bulk.
- Output from evaporation model:
  - u_∞: Vapor velocity outside Knudsen layer, in the frame of the interface.
  - T_∞: Vapor temperature outside Knudsen layer.

Given that the ideal gas law applies, we may from this output find other interesting macroscopic properties such as density (ρ_∞) and evaporation mass flux (j),

$$\rho_\infty = \frac{p_\infty}{RT_\infty}, \tag{3}$$

$$j = \rho_\infty u_\infty. \tag{4}$$

Here R is the gas constant per unit mass ($R = R_0/M$), R_0 is the universal gas constant, and M is the molecular mass. An important point to note is that when T_l and p_∞ are specified, one does not get the liberty of specifying T_∞ independently. Instead T_∞ is an output of the evaporation model, and becomes a boundary condition imposed on the macroscopic problem.

The pressure in the liquid bulk is relatively close to that of the vapor bulk, p_∞, but this will depend on surface curvature (surface tension) and evaporation rate (vapor thrust). In any case, the liquid bulk pressure does not actually enter into the following calculations. What does enter into the calculations from the liquid side is the temperature T_l and the corresponding saturation pressure, $p_\mathrm{s}(T_\mathrm{l})$. As we shall see, the difference between this saturation pressure and the pressure imposed from the vapor (p_∞) is in fact the driving force behind evaporation.

2.2. Thermodynamic states and the saturation line

The models developed herein will make reference to the *saturation line*. This is the line in pressure–temperature space separating the liquid region and the vapor region of a pure fluid. When a state is exactly on this line the state is *saturated*. The saturation line is a property of equilibrium thermodynamics, and an appropriate thermodynamic model for the fluid in question can supply the functions $p_\mathrm{s}(T)$, and its inverse $T_\mathrm{s}(p)$, for this line. The slope of the saturation line at a given temperature may be approximated through the Clausius–Clapeyron equation,

$$\frac{\mathrm{d}p_\mathrm{s}(T)}{\mathrm{d}T} = \frac{L\rho_\mathrm{s}(T)}{T}, \tag{5}$$

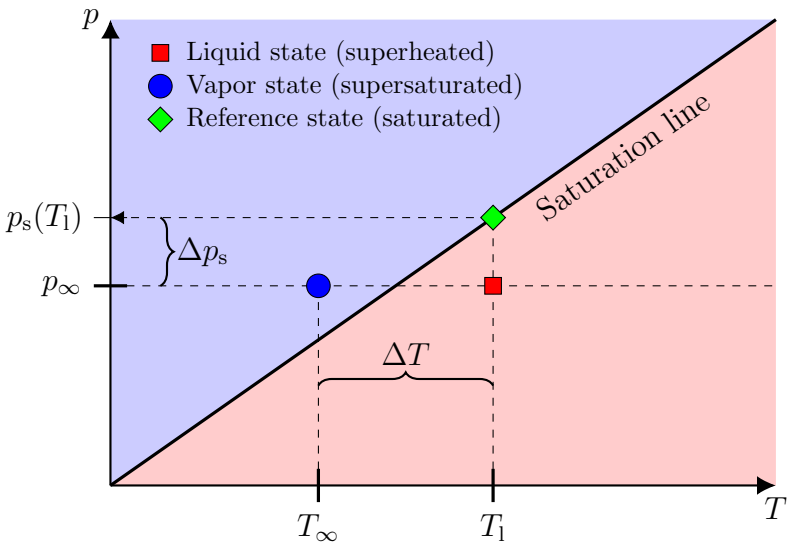

Figure 2: An illustration of the actual liquid and vapor states and the unrealized reference state $p_s(T_l)$, in relation to the saturation line. For the purposes of this sketch the liquid bulk pressure has been assumed to be very close to the vapor bulk pressure. Also, in this example the vapor is supersaturated, but that need not always be the case.

where L is the latent heat and $\rho_s(T)$ is the saturated vapor density.

The models herein importantly make use of a *reference state* which has the same temperature as the liquid and a pressure equal to the corresponding saturation pressure $p_s = p_s(T_l)$. Note that this state is not actually realized anywhere in the system, but its properties will be used to calculate the evaporation flux.

The actual states of liquid and the vapor on either side of the Knudsen layer are not in general on the saturation line. The liquid state is always superheated in the case of evaporation, while the vapor state may be either supersaturated or superheated, depending on conditions. The relationships between the states and the saturation line are illustrated in Fig. 2. In particular this illustration shows the *driving parameter* for evaporation,

$$\Delta p_s = p_s(T_l) - p_\infty, \tag{6}$$

which is not a realized pressure jump, but rather the difference between reference state pressure and actual imposed pressure. Fig. 2 also shows the difference

$$\Delta T = T_l - T_\infty, \tag{7}$$

which is an actual realized temperature jump, seen as a discontinuity on the macroscopic scale due to the much smaller scale of the Knudsen layer. Note that ΔT is the total temperature difference from the liquid bulk (T_l) to the vapor bulk (T_∞), not just the temperature difference across the Knudsen layer ($T_0 - T_\infty$). Note also that, as discussed in Ytrehus (1997, Sec. 6.3), the latter is only a small fraction ($\approx 8\%$) of the total temperature jump. The majority of the temperature jump occurs across the very thin interface transition at $z = 0$ ($T_l - T_0$).

In order to quantify the relations between these states, and obtain practical results such as the resulting evaporation flux, it is necessary to resort to evaporation models like the ones provided by kinetic theory.

2.3. Kinetic theory background

In kinetic theory we deal with the dynamics of velocity distribution functions $f(\boldsymbol{x}, t, \boldsymbol{\xi})$, where $\boldsymbol{x}$ is position, t is time, and $\boldsymbol{\xi}$ is a molecular velocity vector. The distribution represents the number of molecules at a given point $(\boldsymbol{x}, t)$ having a specific velocity. In technical terms, $f\mathrm{d}^3\boldsymbol{\xi}$ gives the number density of particles within the element of velocity space $\mathrm{d}^3\boldsymbol{\xi}$. An important form of f is the (drifting) *Maxwellian* distribution

$$f_M(\boldsymbol{\xi}; T, n, u) = \frac{n}{(2\pi RT)^{3/2}} \exp\left(-\frac{(\boldsymbol{\xi} - u\hat{\boldsymbol{z}})^2}{2RT}\right), \tag{8}$$

which describes how the particles in an ideal gas of total number density ($n = p/(k_B T)$) and bulk flow speed u along the z-axis will distribute across the possible velocity states if allowed to relax to equilibrium.

All the following kinetic-theory evaporation models share a fundamental postulate that makes important use of Eq. (8). This postulate is that the flux of evaporating particles from the liquid surface into the Knudsen layer may be described by the outgoing half of the Maxwellian distribution corresponding to the reference state.

It will be crucial to express the total fluxes of mass, momentum and energy associated with the Maxwellian. We define the functions Ψ_i,

$$\Psi = (m, m\xi_z, \frac{1}{2}m\boldsymbol{\xi}^2), \tag{9}$$

which are the mass, z-momentum and kinetic energy of a molecule, respectively. The net fluxes into the $z > 0$ half-plane due to the Maxwellian are

$$\int_{\xi_z>0} \xi_z \Psi_i f_\mathrm{M} \mathrm{d}\boldsymbol{\xi} = \begin{cases} \rho\sqrt{\frac{RT}{2\pi}} F^+(S) & , \quad i=1 \\ \rho\frac{RT}{2} G^+(S) & , \quad i=2 \\ 2\rho RT\sqrt{\frac{RT}{2\pi}} H^+(S) & , \quad i=3 \end{cases} \tag{10}$$

and the net fluxes into the $z < 0$ half-plane are

$$\int_{\xi_z<0} \xi_z \Psi_i f_\mathrm{M} \mathrm{d}\boldsymbol{\xi} = \begin{cases} -\rho\sqrt{\frac{RT}{2\pi}} F^-(S) & , \quad i=1 \\ \rho\frac{RT}{2} G^-(S) & , \quad i=2 \\ -2\rho RT\sqrt{\frac{RT}{2\pi}} H^-(S) & , \quad i=3 \end{cases} . \tag{11}$$

Here we have defined the dimensionless *speed ratio*,

$$S(u,T) = \frac{u}{\sqrt{2RT}}, \tag{12}$$

which compares the macroscopic flow speed (u) to the average molecular speed of the stationary Maxwellian ($\sim \sqrt{RT}$). Note that since the speed-of-sound of a monatomic ideal gas is $\sqrt{(5/3)RT}$, the Mach number is simply $\sqrt{(6/5)}S$.

The functions $F^\pm(S)$, $G^\pm(S)$ and $H^\pm(S)$ all approach unity for small S, and are fully defined in Eqs. (A.1) to (A.3) of Appendix A.

2.4. Hertz–Knudsen (HK) formula

Hertz (1882) and Knudsen (1915) considered a case of molecular exchange between two opposing stationary surfaces, under high-vacuum conditions so that the exchange is essentially free molecular flow without collisions. The model assumes that both surfaces eject molecules according to the inwards-facing half of the Maxwellian distribution corresponding to their temperature and some density, and that these molecules reach the other surface undisturbed.

When applied to the present context shown in Fig. 1, one surface is the liquid surface at T_l and the other surface is the boundary of the bulk vapor outside the Knudsen layer at T_∞. This means that the liquid surface ejects molecules according to the $\xi_z > 0$ half of the distribution

$$f_\mathrm{e} = f_\mathrm{M}(T_\mathrm{l}, n_\mathrm{e}, 0), \tag{13}$$

and that the outer boundary of the Knudsen layer sends back molecules according to the $\xi_z < 0$ half of the distribution

$$f_\infty = f_\mathrm{M}(T_\infty, n_\infty, 0). \tag{14}$$

Here n_e and n_∞ are the total number densities of the reference state and the bulk vapor state (p_∞, T_∞), respectively. If we add these two contributions, use Eqs. (10) and (11), and introduce an *evaporation/condensation coefficient* $\alpha \in [0,1]$ as an unknown pre-factor, the following net evaporation flux is found:

$$\begin{aligned} j &= \alpha \left[\int_{\xi_z>0} \xi_z \Psi_1 f_\mathrm{e} \mathrm{d}\boldsymbol{\xi} + \int_{\xi_z<0} \xi_z \Psi_1 f_\infty \mathrm{d}\boldsymbol{\xi} \right], \\ &= \alpha \left[\frac{p_\mathrm{s}(T_\mathrm{l})}{\sqrt{2\pi RT_\mathrm{l}}} - \frac{p_\infty}{\sqrt{2\pi RT_\infty}} \right]. \end{aligned} \tag{15}$$

While the Hertz-Knudsen model captures some of the correct qualitative features, it is inadequate for the following two reasons:

- The incoming Maxwellian f_∞ has u_∞ set to zero, even though under realistic evaporation conditions the state outside the Knudsen layer must have a non-zero drift.
- The model only considers conservation of mass, and ignores conservation of momentum and energy.

The usage of the formula in Eq. (15) requires the input of T_∞. This model is unable to make an independent prediction for the downstream vapor temperature, so in order to arrive at a practically useful model we must make an additional ad-hoc assumptions. This is the assumption of saturated downstream vapor, i.e.

$$T_\infty = T_\mathrm{s}(p_\infty), \tag{16}$$

which for weak evaporation (small Δp_s and ΔT) transforms Eq. (15) to

$$j = \alpha \left[1 - \frac{1}{2}\frac{RT_\mathrm{l}}{L} \right] \frac{\Delta p_\mathrm{s}}{\sqrt{2\pi RT_\mathrm{l}}}. \tag{17}$$

This is a practically usable model whose inputs are the known liquid temperature T_l, the outside pressure p_∞, and the saturation-line function $p_\mathrm{s}(T)$.

2.5. Schrage–Mills (SM) formula

Schrage (1953) improved on the Hertz–Knudsen model by addressing the first of the two issues listed earlier. This involves taking into account the nonzero u_∞ in the incoming Maxwellian,

$$f_\infty = f_\mathrm{M}(T_\infty, n_\infty, u_\infty). \tag{18}$$

Following the same argument as before, this leads to the net evaporation flux

$$\begin{aligned} j &= \alpha \left[\int_{\xi_z>0} \xi_z \Psi_1 f_\mathrm{e} \mathrm{d}\boldsymbol{\xi} + \int_{\xi_z<0} \xi_z \Psi_1 f_\infty \mathrm{d}\boldsymbol{\xi} \right], \\ &= \alpha \left[\frac{p_\mathrm{s}(T_\mathrm{l})}{\sqrt{2\pi RT_\mathrm{l}}} - \frac{p_\infty}{\sqrt{2\pi RT_\infty}} F^-(S_\infty) \right], \end{aligned} \tag{19}$$

where $S_\infty = S(u_\infty, T_\infty)$. Unfortunately, Eq. (19) is actually an implicit equation for j since S_∞ depends on j.

However, we may solve for j by assuming that the evaporation is weak, in the sense that

$$S_\infty \ll 1. \tag{20}$$

This allows us to expand $F^-(S_\infty)$ for small S_∞ according to Eq. (A.1), which leads to the more useful Schrage-Mills formula (Mills, 1995),

$$j = \frac{\alpha_\mathrm{e}}{1-\frac{1}{2}\alpha_\mathrm{e}}\left[\frac{p_\mathrm{s}(T_\mathrm{l})}{\sqrt{2\pi R T_\mathrm{l}}} - \frac{p_\infty}{\sqrt{2\pi R T_\infty}}\right]. \tag{21}$$

Besides having a different pre-factor, this is identical to the main Hertz–Knudsen result in Eq. (15).

Just as with the Hertz–Knudsen model, we may further linearize Eq. (21) and assume saturated vapor in order to arrive at the more convenient formula

$$j = \frac{\alpha_\mathrm{e}}{1-\frac{1}{2}\alpha_\mathrm{e}}\left[1 - \frac{1}{2}\frac{RT_\mathrm{l}}{L}\right]\frac{\Delta p_\mathrm{s}}{\sqrt{2\pi R T_\mathrm{l}}}. \tag{22}$$

2.6. Boltzmann Equation Moment Method (BEMM) model

Both the Hertz–Knudsen (HK) and the Schrage–Mills (SM) models have one major issue in common: They only consider conservation of mass, and not conservation of momentum and energy. The result of this is that they contain insufficient information to predict the temperature of the downstream vapor (T_∞).

The Boltzmann Equation Moment Method (BEMM) model is a way of resolving this issue by considering a wider set of conservation laws across the Knudsen layer. Fundamentally it only requires the general form of the Boltzmann equation, and the knowledge that mass, momentum and energy are conserved in individual molecular collisions, regardless of the details of the process. These are the so-called *collision invariants*, which lead to three conservation equations for the Knudsen layer that must be solved simultaneously to find macroscopic properties such as the evaporation mass flux. The derivation of the BEMM equations herein is a concise summary of what is covered in greater detail in Ytrehus (1997).

2.6.1. The Boltzmann Equation

The BEMM models are based on the 1D steady state version of the fundamental Boltzmann equation of kinetic theory (Cercignani, 1988) to describe the gas in the Knudsen layer. The equation reads

$$\xi_z \frac{\partial f}{\partial z} = Q(ff_1), \tag{23}$$

which is an integro-differential equation for the scalar velocity distribution function $f(z,\boldsymbol{\xi})$. While the left hand side is a straightforward advection type term, the right hand side $Q(ff_1)$ is the collisional rate of change of f. This generally involves an integral over all possible binary collisions that either scatters out or scatters into the velocity state in question.

2.6.2. Boundary conditions of the Knudsen layer

In addition to the governing equation Eq. (23), we also need boundary conditions for the distribution function $f(z,\boldsymbol{\xi})$ at either side of the Knudsen layer in Fig. 1. Generally the conditions at the liquid surface cannot be found from within the scope of kinetic theory itself, but requires more detailed descriptions of the dense phase and its surface. However, as will be shown below, this issue is resolved in the moment method by making a set of crucial assumptions regarding the function $f(z,\boldsymbol{\xi})$.

As before, the outer edge of the Knudsen layer ($z\to\infty$) has a drifting Maxwellian distribution according to the bulk vapor state,

$$f(\infty,\boldsymbol{\xi}) \equiv f_\infty(\boldsymbol{\xi}) = f_\mathrm{M}(\boldsymbol{\xi}; T_\infty, n_\infty, u_\infty), \tag{24}$$

where $f_\infty(\boldsymbol{\xi})$ is now a shorthand for this specific Maxwellian state. The main challenge relates to determining the vapor state at the liquid surface ($z=0$), which from now on is denoted by the shorthand $f_0(\boldsymbol{\xi})$,

$$f_0(\boldsymbol{\xi}) \equiv f(0,\boldsymbol{\xi}). \tag{25}$$

In the moment method this challenge is met by making certain assumptions regarding the form of the molecular distribution function throughout the Knudsen layer, i.e. how $f(z,\boldsymbol{\xi})$ changes as a function of z. This involves representing the incoming ($\xi_z<0$) or outgoing ($\xi_z>0$) parts of full distributions, and these will generally be labeled as f^- and f^+, respectively. Specifically we make the *ansatz* that $f(z,\boldsymbol{\xi})$ is a linear combination of three distributions (Ytrehus, 1977): The outgoing distribution at the interface (f_0^+), the outgoing distribution outside the Knudsen layer (f_∞^+) and the incoming distribution outside the Knudsen layer (f_∞^-). We write this as

$$\begin{aligned} f(z,\boldsymbol{\xi}) = {} & a_\mathrm{e}^+(z) f_0^+(\boldsymbol{\xi}) \\ & + a_\infty^+(z) f_\infty^+(\boldsymbol{\xi}) \\ & + a_\infty^-(z) f_\infty^-(\boldsymbol{\xi}), \end{aligned} \tag{26}$$

with the z-dependent coefficients having the following boundary conditions,

$$\begin{array}{lll} & a_\mathrm{e}^+ = 1 & \qquad\qquad a_\mathrm{e}^+ = 0 \\ z=0: & a_\infty^+ = 0 & z\to\infty: \quad a_\infty^+ = 1. \\ & a_\infty^- = \beta & \qquad\qquad a_\infty^- = 1 \end{array} \tag{27}$$

Here β is a new parameter linked to the unknown incoming distribution, which will be determined along with the others from the ensuing moment equations based on the Boltzmann equation. Note how Eq. (26) with Eq. (27) satisfies Eq. (24) directly, and leads to

$$f_0(\boldsymbol{\xi}) = f_0^+(\boldsymbol{\xi}) + \beta f_\infty^-(\boldsymbol{\xi}), \tag{28}$$

for the left-hand boundary condition.

We then assume that the outgoing distribution at the interface is a combination of an *emission* part and a *reflection* part,

$$f_0^+(\boldsymbol{\xi}) = \alpha_\mathrm{e} f_\mathrm{e}^+(\boldsymbol{\xi}) + (1-\alpha_\mathrm{c}) f_\mathrm{r}^+(\boldsymbol{\xi}), \tag{29}$$

where f_e is the same emission distribution as before, Eq. (13), and where f_r is a reflection distribution to be estimated later. In Eq. (29) we have used an ad-hoc weighing which introduces an evaporation-coefficient ($\alpha_e \in [0,1]$) and a condensation-coefficient ($\alpha_c \in [0,1]$).

The outgoing reflection distribution f_r^+ in Eq. (29) is assumed to be the outgoing part of a Maxwellian distribution at the liquid temperature, but with a different unknown number density n_r,

$$f_r^+(\boldsymbol{\xi}) = f_M^+(\boldsymbol{\xi}; T_l, n_r, 0). \tag{30}$$

The number density n_r can now be found through the *flux-condition*, which states that the ideal ($\alpha_c \to 0$) reflected mass flux is equal to the incoming mass flux at the same location. When combining this principle with Eq. (28), it may be written as

$$\int_{\xi_z>0} \xi_z f_r^+ \mathrm{d}\boldsymbol{\xi} = \beta \int_{\xi_z<0} |\xi_z| f_\infty^- \mathrm{d}\boldsymbol{\xi}. \tag{31}$$

According to Eq. (24) and Eq. (30), both distributions in Eq. (31) are Maxwellian distributions, and thus we may use Eqs. (10) and (11) to evaluate the integrals. This simplifies the flux-condition to a relation between the densities n_r and n_∞,

$$n_r \sqrt{\frac{RT_l}{2\pi}} = \beta \sqrt{\frac{RT_\infty}{2\pi}} F^-(S_\infty) n_\infty. \tag{32}$$

By combining Eqs. (28) to (30) we finally find that the $z = 0$ boundary condition may be written as

$$f(0,\boldsymbol{\xi}) = \begin{cases} \left(\alpha_e + (1-\alpha_c)\frac{n_r}{n_e}\right) f_e^+ & \xi_z > 0 \\ \beta f_\infty^- & \xi_z < 0 \end{cases} \tag{33}$$

with n_r given according to Eq. (32). Of course, this boundary condition depends on the new unknown β that we have introduced, in accordance with the basic requirement that $f(0,\boldsymbol{\xi})$ (for $\boldsymbol{\xi} < 0$) is an outcome of the solution.

We now have both a governing equation Eq. (23) and boundary conditions Eqs. (24) and (33) for the distribution function $f(z,\boldsymbol{\xi})$ in the Knudsen layer. There are several possible ways to find a solution to this problem, but so far only the moment method has led to (approximate) analytical results in the non-linear regime. This approach is demonstrated in the next part.

2.6.3. The moment method

Obtaining a detailed solution of Eq. (23) across the Knudsen layer requires the choice of a specific collision model for $Q(ff_1)$. However, in the present case where only boundary properties such as the speed and temperature of the downstream vapor are of interest, this is not necessary. Instead, it is sufficient to state that mass, z-momentum and energy are collision-invariants. This may be formally stated in terms of the quantities Ψ_i in Eq. (9) as

$$\int \Psi_i(\boldsymbol{\xi}) Q(ff_1) \mathrm{d}\boldsymbol{\xi} = 0, \quad (i = 1,2,3), \tag{34}$$

and this will lead to the governing equations of the moment method. If we multiply the Boltzmann equation Eq. (23) by Ψ_i, integrate throughout velocity space, and use what we know about collision invariants from Eq. (34), we get

$$\frac{\partial}{\partial z} \int \Psi_i(\boldsymbol{\xi}) \xi_z f(z,\boldsymbol{\xi}) \mathrm{d}\boldsymbol{\xi} = 0, \quad (i = 1,2,3). \tag{35}$$

In words, this means that these integrals (moments) are independent of z, and therefore must have the same value of either side of the Knudsen layer. If we then use the boundary conditions Eqs. (24) and (33) to split the integrals into outgoing and ingoing parts, and use Eqs. (10) and (11) to evaluate the half-space integrals, we get the following conservation equations

$$\alpha_e \mathcal{Z}\sqrt{\mathcal{Y}} + (1-\alpha_c)\beta F^- - \beta F^- = 2\sqrt{\pi} S_\infty \tag{36}$$

$$\alpha_e \mathcal{Z} + (1-\alpha_c)\sqrt{\frac{1}{\mathcal{Y}}}\beta F^- + \beta G^- = 4S_\infty^2 + 2 \tag{37}$$

$$\alpha_e \mathcal{Z} + (1-\alpha_c)\sqrt{\frac{1}{\mathcal{Y}}}\beta F^- - \sqrt{\mathcal{Y}}\beta H^- = \sqrt{\mathcal{Y}}\sqrt{\pi} S_\infty \left(S_\infty^2 + \frac{5}{2}\right) \tag{38}$$

for mass, momentum and energy, respectively. Here it is implicit that F^-, G^- and H^- are evaluated at $S = S_\infty$, and we have defined the dimensionless ratios

$$\mathcal{Z} = \frac{p_s(T_l)}{p_\infty}, \tag{39}$$

$$\mathcal{Y} = \frac{T_\infty}{T_l}. \tag{40}$$

We now have three equations, Eqs. (36) to (38), for the four variables S_∞, $\mathcal{Z}$, $\mathcal{Y}$ and β. Thus, we are free to impose one of them and solve for the remaining three. In the present case we impose a pressure-based driving force $\mathcal{Z}$ and solve for the remaining three variables. Based on such a solution the evaporation mass flow rate may be found as

$$\begin{aligned} j &= \rho_\infty u_\infty \\ &= \frac{p_\infty}{\sqrt{RT_\infty}} \sqrt{2} S_\infty \\ &= \frac{p_\infty}{\sqrt{RT_l}} \sqrt{\frac{2}{\mathcal{Y}}} S_\infty. \end{aligned} \tag{41}$$

The gas kinetic convection problem contained within Eqs. (36) to (38) reflects a fundamental element in any solution to the half-space problem of the steady 1D Boltzmann equation; namely that some relations must exist between the downstream variables n_∞, u_∞ T_∞ and the boundary condition at the interface; in our case Eq. (33). Furthermore, in our case these conditions do not depend upon the specific collision model for $Q(ff_1)$, since Eqs. (36) to (38) are derived from conservation equations only. The results, for instance mass flux versus speed ratio S_∞, have been compared with BGK-solutions, Monte Carlo simulations and experiments (Ytrehus, 1997, Fig. 10 pp. 253),

and a maximum deviation of 2% is observed close to the sonic point. This matter has been revisited more recently by Frezzotti (2007), pointing out that the moment method seems to slightly overestimate the back-scattered molecules. This has the effect of reducing the net mass flux somewhat, again in the vicinity of sonic downstream conditions.

2.6.4. Linearization

The nonlinear conservation equations, Eqs. (36) to (38), must be solved numerically. It can be very convenient to have an analytical solution instead, and this can be achieved by linearizing in the case of weak evaporation. We define new quantities $\Delta\mathcal{Z}$, $\Delta\mathcal{Y}$ and $\Delta\beta$ as the deviations from unity of the corresponding quantities,

$$\mathcal{Z} = 1 + \Delta\mathcal{Z}, \tag{42}$$
$$\mathcal{Y} = 1 - \Delta\mathcal{Y}, \tag{43}$$
$$\beta = 1 + \Delta\beta, \tag{44}$$

so that $\Delta\mathcal{Z} = (p_\mathrm{s}(T_\mathrm{l}) - p_\infty)/p_\infty$ and $\Delta\mathcal{Y} = (T_\mathrm{l} - T_\infty)/T_\mathrm{l}$. We then assume weak evaporation, in the sense that

$$S_\infty \ll 1, \quad \Delta\mathcal{Z} \ll 1, \quad \Delta\mathcal{Y} \ll 1, \quad \Delta\beta \ll 1. \tag{45}$$

By applying the common simplification (Ytrehus, 1997)

$$\alpha_\mathrm{c} = \alpha_\mathrm{e} = \alpha, \tag{46}$$

and using the expansions of F^-, G^- and H^- for small S, shown in Appendix A, the first-order approximate solution may then be found as

$$\Delta\mathcal{Y} = \frac{\sqrt{\pi}}{4} S_\infty, \tag{47}$$
$$\Delta\beta = \sqrt{\pi}\left[\frac{2}{\pi} - \frac{9}{16}\right] S_\infty, \tag{48}$$
$$\Delta\mathcal{Z} = \frac{32\pi + 32\alpha - 23\pi\alpha}{16\sqrt{\pi}\alpha} S_\infty. \tag{49}$$

One may solve Eq. (49) for S_∞ to get the important result

$$S_\infty = \frac{1}{2\sqrt{\pi}} \left(\frac{\alpha}{1 - \left(\frac{\gamma-1}{\gamma}\right)\alpha} \right) \Delta\mathcal{Z}. \tag{50}$$

with the shorthand γ defined as

$$\gamma = \frac{32\pi}{32 + 9\pi} \approx 1.67. \tag{51}$$

From Eq. (41) and Eq. (50) we may now find the evaporation mass flux as

$$j = \left(\frac{\alpha}{1 - \left(\frac{\gamma-1}{\gamma}\right)\alpha} \right) \frac{\Delta p_\mathrm{s}}{\sqrt{2\pi R T_\mathrm{l}}} \tag{52}$$

which may be directly compared to the final HK and SM results in Eqs. (17) and (22). The solutions obtained from this linearized BEMM model will be referred to as BEMM(L).

With the BEMM model and its linearization, as opposed to in the HK and SM models, we obtain predictions for the downstream vapor temperature T_∞. From the linearized results Eq. (47) and Eq. (50) we may find that the relative temperature jump is proportional to the driving force as

$$\frac{T_\mathrm{l} - T_\infty}{T_\mathrm{l}} = \Delta\mathcal{Y} = \frac{1}{8} \left(\frac{\alpha}{1 - \left(\frac{\gamma-1}{\gamma}\right)\alpha} \right) \Delta\mathcal{Z}. \tag{53}$$

and thus also proportional to the evaporation rate.

Based on Eq. (53) we may investigate where the state of the downstream vapor lies in relation to the saturation line. According to the Clausius–Clapeyron relation, Eq. (5), if the vapor state is on the saturation line the temperature jump must be approximately $\Delta\mathcal{Y} = (RT_\mathrm{l}/L)\Delta\mathcal{Z}$. If the actual temperature jump is greater than this, the vapor is supersaturated. If it is smaller, the vapor is superheated. By comparing this with the result in Eq. (53) we find that

$$8\left[\frac{1}{\gamma} + \frac{1-\alpha}{\alpha}\right] \quad \begin{cases} < \frac{L}{RT_\mathrm{l}} & \text{Supersaturated} \\ > \frac{L}{RT_\mathrm{l}} & \text{Superheated} \end{cases}. \tag{54}$$

Since Trouton's rule states that $RT_\mathrm{l}/L \approx 0.1$, we may within this approximation conclude that $\alpha > 0.6$ leads to supersaturated vapor and that $\alpha < 0.6$ leads to superheated vapor. Since water at its atmospheric boiling point has $RT_\mathrm{l}/L \approx 1/13$, it has the transition at $\alpha \approx 0.5$ instead.

The actual value of α is subject to much debate (Persad and Ward, 2016), but as discussed in Aursand et al. (2018) it can likely be expected to be in the range of 0.7–1.0 for moderate evaporation. However, the presence of impurities at the interface may lower the value significantly, all the way down to the order of 0.1 (Ytrehus, 1997).

It is worth noting that the above results are in principle restricted to monatomic substances only. However, polyatomic effects in evaporation have been considered by Cercignani (1981), and in the linearized version of his results the simple mass flow formula Eq. (52) is recovered. Hence, internal degrees of freedom do not affect the most basic outcome of the theory in the linear regime.

2.7. Comparison of evaporation models

In order to summarize and compare models it is useful to have a dimensionless measure of the resulting evaporation rate. One such measure is the downstream speed-ratio S_∞, as defined by Eq. (12) with $S = S(u_\infty, T_\infty)$. This is the bulk outgoing speed of the downstream vapor relative to the average molecular speed of a vapor at that temperature. Within the weak evaporation limit, which they were derived with in the first place, all the linearized models may be written on the form

$$S_\infty = \frac{r(\alpha)\phi(T_\mathrm{l})}{\sqrt{4\pi}} \Delta\mathcal{Z}. \tag{55}$$

The pre-factors r and ϕ depend on the specific model, according to

$$r_{\mathrm{HK}} = \alpha, \qquad r_{\mathrm{SM}} = \frac{\alpha}{1 - \frac{1}{2}\alpha}, \tag{56}$$

$$r_{\mathrm{BEMM}} = \frac{\alpha}{1 - \left(\frac{\gamma-1}{\gamma}\right)\alpha}, \tag{57}$$

and

$$\phi_{\mathrm{HK}} = \phi_{\mathrm{SM}} = 1 - \frac{1}{2}\frac{RT_\mathrm{l}}{L}, \qquad \phi_{\mathrm{BEMM}} = 1. \tag{58}$$

The full nonlinear BEMM model obviously does not fit into the same simple mold. Given a driving force $\mathcal{Z} = 1 + \Delta\mathcal{Z}$, the set of coupled nonlinear equations in Eqs. (36) to (38) must be solved numerically for the three quantities S_∞, $\mathcal{Y}$ and β.

We are now in a position to compare the predictions of four different models: HK, SM, linearized BEMM(L), and full nonlinear BEMM. In the following comparison we treat the pressure-based driving force $\Delta\mathcal{Z}$ as the independent parameter, and compare the results for evaporation rate (S_∞) and temperature jump ($\Delta\mathcal{Y}$). The plots do not go beyond a Mach number of Ma = 1, as it is known that the assumed 1D evaporative flow in the Knudsen layer is restricted to the subsonic regime (Arthur and Cercignani, 1980; Ytrehus, 1997). This is equivalent to a maximum speed ratio of $S \approx 0.91$. The evaporation–condensation coefficient is kept at $\alpha = 1$ for simplicity, and the fluid is assumed to follow Trouton's rule, $RT_\mathrm{l}/L \approx 0.1$. The latter parameter is only necessary for the HK and SM models.

The results for S_∞ are shown in Fig. 3, together with experimental data from Ytrehus (1977) (also shown in Ytrehus (1997, Sec. 4.4)). This provides convincing validation for the nonlinear BEMM model, while clearly showing that the linearization is only a good approximation in the $\Delta\mathcal{Z} \ll 1$ regime. From the data and the BEMM model we see that the supersonic regime is approached at approximately $\Delta\mathcal{Z} \approx 4$. Since the nonlinear BEMM model is both the most advanced model and the model closest to experimental data, we will from now on consider its results as the reference for the purposes of assessing the accuracy of the more crude models.

The results for $\Delta\mathcal{Y}$ are shown in Fig. 4. Note that this includes only the BEMM models, as the HK and SM models are unable to make predictions regarding the downstream vapor state.

In addition to investigating the speed ratio S_∞ of the evaporation, we may also take a direct look at the evaporation mass flux. For this purpose we define a dimensionless evaporation mass flux J^*, using a scale that depends on liquid-side properties only,

$$J^* = \frac{j}{\rho_\mathrm{s}(T_\mathrm{l})\sqrt{\frac{RT_\mathrm{l}}{2\pi}}}. \tag{59}$$

Due to the fact that $\rho_\infty \neq \rho_\mathrm{s}(T_\mathrm{l})$ and $T_\infty \neq T_\mathrm{l}$ in general, J^* does not only depend on S_∞. From Eq. (41) we find

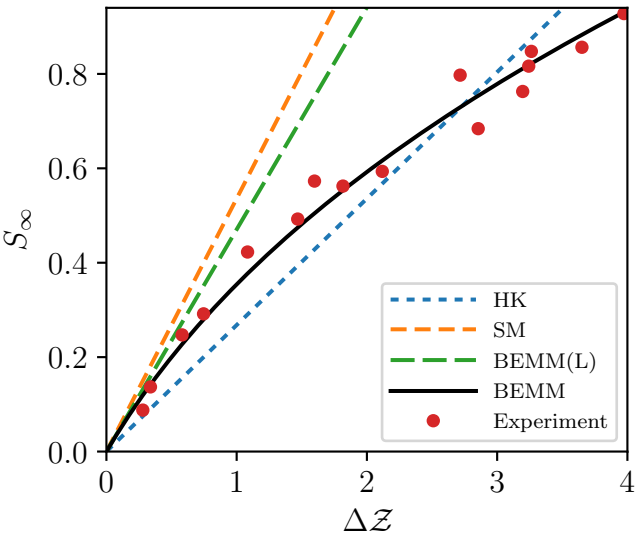

Figure 3: Predicted speed-ratio as a function of driving force $\Delta\mathcal{Z} = \Delta p_\mathrm{s}(T_\mathrm{l})/p_\infty$. Parameters are set to $\alpha = 1$ and $RT_\mathrm{l}/L = 0.1$. Also shown are experimental data from Ytrehus (1977).

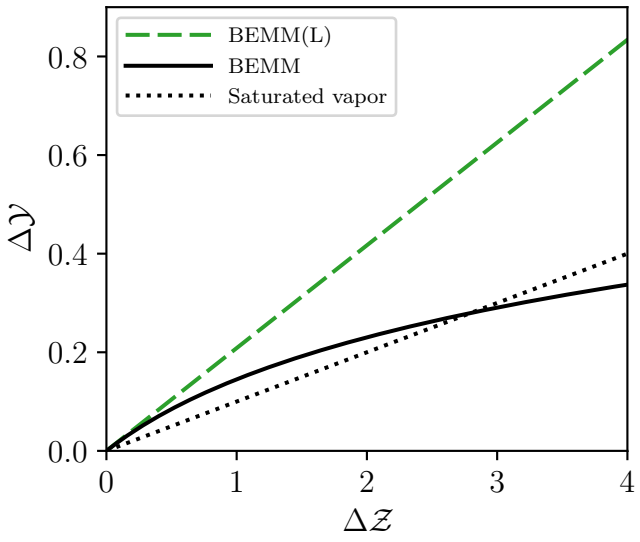

Figure 4: Predicted interface temperature discontinuities, $\Delta\mathcal{Y} = \Delta T/T_\mathrm{l}$, as a function of driving force $\Delta\mathcal{Z} = \Delta p_\mathrm{s}(T_\mathrm{l})/p_\infty$. Also shown is the approximate relationship expected if the downstream vapor is saturated. Parameters are set to $\alpha = 1$ and $RT_\mathrm{l}/L = 0.1$.

that

$$J^* = \frac{\sqrt{4\pi}}{\mathcal{Z}\sqrt{\gamma}} S_\infty. \tag{60}$$

However, for weak evaporation the linearized models yield a simple direct relationship to the driving force $\Delta\mathcal{Z}$,

$$J^* = r(\alpha)\phi(T_\mathrm{l})\Delta\mathcal{Z} \tag{61}$$

A comparison of results for J^* in the weak evaporation regime is shown in Fig. 5. It is clear that the full BEMM model starts deviating from its linearization as soon as $\Delta\mathcal{Z} \ll 1$ is no longer true, and that the linearization error yields an over-prediction. We also see that the SM model gives results quite close to the linear BEMM model, but that the HK model under-predicts the evaporation rate by about a factor of two.

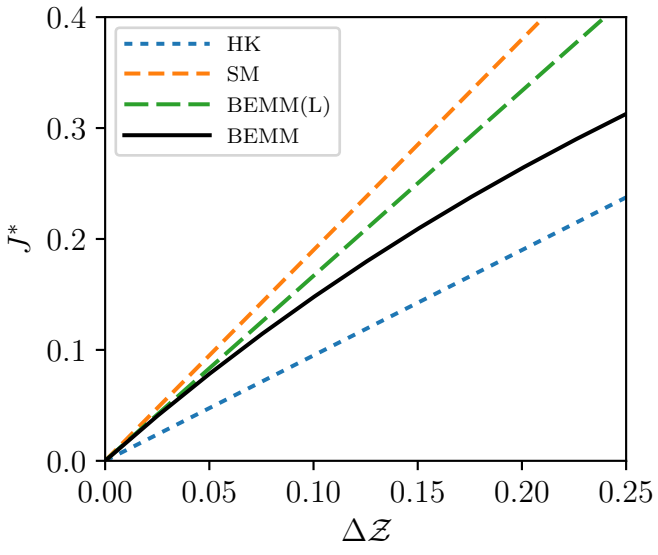

Figure 5: Predicted evaporation rate as a function of driving force $\Delta\mathcal{Z} = \Delta p_\mathrm{s}(T_\mathrm{l})/p_\infty$, in the weak evaporation regime $\Delta\mathcal{Z} \ll 1$. Parameters are set to $\alpha = 1$ and $RT_\mathrm{l}/L = 0.1$.

2.8. Simplification: Linearizing the saturation line

The evaporation models summarized in Sec. 2.7 require the knowledge of the fluid's thermodynamic saturation line, in the form of the function $p_\mathrm{s}(T)$, in order to evaluate the driving force $\Delta\mathcal{Z}$ for a given case. The function $p_\mathrm{s}(T)$ may in practice be represented either by interpolating experimental data or by using a thermodynamic equation of state. However, in cases where the evaporation is weak it may be convenient to represent the real saturation line by a linearization around a known point on the line. Here we choose that point to be $(p_\infty, T_\mathrm{s}(p_\infty))$. Note that this state is not necessarily realized in the system, but is merely another reference state. According to the Clausius–Clapeyron relation, Eq. (5), the function $p_\mathrm{s}(T)$ may then be approximated by

$$p_\mathrm{s}(T) = p_\infty + \frac{L\rho_\mathrm{s}}{T_\mathrm{s}}\left[T - T_\mathrm{s}\right]. \tag{62}$$

where ρ_s and T_s are short-hands for $\rho_\mathrm{s}(p_\infty)$ and $T_\mathrm{s}(p_\infty)$, respectively. This means that the driving force can be approximated as a function of a single variable T_l,

$$\Delta\mathcal{Z} = \frac{L}{RT_\mathrm{s}}\left[\frac{T_\mathrm{l} - T_\mathrm{s}}{T_\mathrm{s}}\right]. \tag{63}$$

The linearized evaporation models may then to first order in $\Delta\mathcal{Z}$ be written on the particularly simple form

$$j = r(\alpha)\frac{\rho_\mathrm{s} L}{\sqrt{2\pi R T_\mathrm{s}}}\left[\frac{T_\mathrm{l} - T_\mathrm{s}}{T_\mathrm{s}}\right], \tag{64}$$

provided that the approximation $\phi \approx 1$ can be made for the HK and SM models. This form is very useful in fluid mechanics contexts where the liquid interface temperature T_l is a variable. If the speed-ratio S_∞ is required, one may simple insert Eq. (63) into Eq. (55). The relation in Eq. (64) is often written as a linear constitutive relation,

$$(T_\mathrm{l} - T_\mathrm{s}) = \frac{\tilde{K}}{r(\alpha)} j, \tag{65}$$

with the constant

$$\tilde{K} = \frac{\sqrt{2\pi R}\, T_\mathrm{s}^{3/2}}{\rho_\mathrm{s} L}. \tag{66}$$

The constant $\tilde{K}$ depends on both fluid properties and applied pressure, and indicates the importance of non-equilibrium evaporation effects. In a sense $\tilde{K}/r$ is an interfacial resistance, indicating how much driving force $(T_\mathrm{l} - T_\mathrm{s})$ is necessary to obtain an evaporation flux (j). The constitutive form in Eq. (65) has been used in thin-film flow modeling by authors such as Burelbach et al. (1988), Panzarella et al. (2000) and Aursand et al. (2018).

3. Case: Evaporating liquid film

3.1. Problem definition

We consider a liquid thin-film that evaporates due to contact with a heated horizontal solid surface. The position of the liquid–vapor interface is described by the film-thickness function $h(x,t)$. A case is defined by fluid properties, an initial uniform film thickness h_0, a wall temperature (T_w) and a vapor bulk pressure (p_∞). Both liquid and vapor consist of the same pure fluid. The case is illustrated in Fig. 6. Note that in this context, the origin of the coordinate is stationary with respect to the solid surface, and no longer follows the liquid–vapor interface.

The goal is to solve the local evaporation-problem along the interface, which yields the two interface temperatures on the liquid and vapor side (T_l and T_∞), the resulting

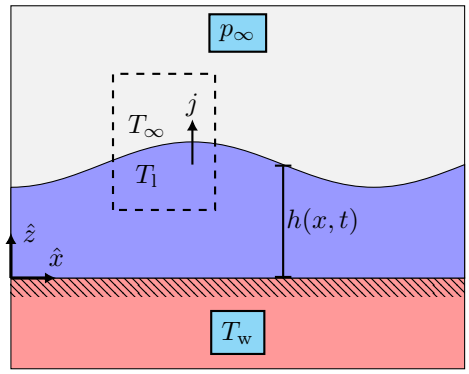

Figure 6: Illustration of the case of an evaporating liquid thin-film confined between a heated solid wall and a vapor. Position is given by the variables x and z, which are directed according to the unit vectors $\hat{\boldsymbol{x}}$ and $\hat{\boldsymbol{z}}$, respectively. A case is defined by the fluid properties, the initial uniform film thickness h_0, the wall temperature (T_w) and the pressure in the vapor bulk (p_∞). The dashed rectangle indicates the domain of the evaporation-problem considered thus far, which here couples to the evolution of the film-thickness function $h(x,t)$.

evaporation mass flux (j), and based on this the evolution of the film-thickness. To keep consistency with the description of the evaporation model, we continue to use T_l and T_∞ to refer to the interface temperatures on the liquid and vapor sides, respectively. The variable temperature within the liquid phase is described by the function T without any subscript.

On the scale of Fig. 6, the entire structure of the finite interface and the Knudsen layer in Fig. 1 is hidden at $z \approx h(x,t)$. However, the fact that the liquid film is very thick compared to the Knudsen layer does not necessarily mean that kinetic-theory effects are irrelevant at this scale. The evaporation models from Sec. 2 couple to the macroscopic model by providing the necessary relations between the evaporation mass flux, applied pressure and liquid-side interface temperature.

Note that for the evaporation models from Sec. 2 to be applicable to wavy interfaces like the one illustrated in Fig. 6, it is necessary that the spatial and temporal scales of the waves are much larger than those of the gas molecules above. Specifically, this requires that the mean free path is much smaller than the wavelength, and that the mean free time is much smaller than the period.

3.2. Continuum model

Based on the case parameters we may define the characteristic temperature difference across the liquid film,

$$\Delta T_\mathrm{w} = T_\mathrm{w} - T_\mathrm{s}. \tag{67}$$

where T_s is a shorthand for $T_\mathrm{s}(p_\infty)$, and thus constant as long as p_∞ is constant. This quantity is used to define the dimensionless temperature (θ),

$$\theta = \frac{T - T_\mathrm{s}}{\Delta T_\mathrm{w}}, \tag{68}$$

which means that the wall has a temperature $\theta = 1$, and that the liquid–vapor interface has a temperature $\theta \approx 0$ due to it being relatively close to saturation. We use h_0 as a scale for film thickness and z-position, giving dimensionless equivalents $H = h/h_0$ and $Z = z/h_0$, respectively. We define the dimensionless mass flux $J = j/j_0$ according to the latent heat and a simple quasi-equilibrium energy balance,

$$j_0 = \frac{k_\mathrm{l} \Delta T_\mathrm{w}}{h_0 L}, \tag{69}$$

where k_l is the thermal conductivity of the liquid. According to Oron et al. (1997, Eq. 2.57), the energy equation in thin liquid films may then be approximated as

$$\frac{\partial^2 \theta}{\partial Z^2} = 0. \tag{70}$$

Also, according to Oron et al. (1997, Eq. 2.86a), the energy balance at the evaporating interface may be approximated as

$$\left.\frac{\partial \theta}{\partial Z}\right|_{Z=H} = -J. \tag{71}$$

A combination of Eqs. (70) and (71) yields

$$J = \frac{1 - \theta_\mathrm{l}}{H}, \tag{72}$$

where θ_l is the dimensionless liquid temperature at the interface ($Z = H$). The relation in Eq. (72) is a single equation with three unknowns H, J and θ_l. In order to solve the problem for a given film thickness H we need an additional relation between these variables, and this is provided by the evaporation model.

3.2.1. Quasi-equilibrium

As a point of comparison for the models based on kinetic theory, we use the quasi-equilibrium approximation. This is an approximation commonly used in computational fluid dynamics (CFD), and is technically only valid in the limit of very weak evaporation. It is equivalent to assuming that the interface temperature is continuous and exactly equal to the saturation temperature,

$$\theta_\mathrm{l} = \theta_\infty = 0. \tag{73}$$

When combined with Eq. (72), this means that the evaporation mass flux is simply given by

$$J_\mathrm{QE} = \frac{1}{H}. \tag{74}$$

This approximation has the issue that J diverges as H approaches zero, something which will not be the case with the non-equilibrium models. It also locks the interface to the saturation temperature by definition, so it is not possible to predict the resulting interface superheat (θ_l).

3.2.2. Kinetic theory models

In Sec. 2 we developed models for the evaporation rate, in terms of S_∞, given a known pressure-based driving force, $\Delta\mathcal{Z}$. However, the present case illustrated in Fig. 6 does not have $\Delta\mathcal{Z}$ as a given parameter. Instead, in this case the evaporation is ultimately driven by the fact that the wall temperature is above the fluid's ambient-pressure saturation temperature, $T_\mathrm{w} > T_\mathrm{s}(p_\infty)$. We denote the dimensionless measure of this driving force by Ω,

$$\Omega = \frac{\Delta T_\mathrm{w}}{T_\mathrm{s}} \tag{75}$$

If we introduce two additional fluid constants,

$$K = \frac{\tilde{K} k_\mathrm{l}}{h_0 L}, \tag{76}$$

and

$$\Gamma = \frac{R T_\mathrm{s}}{L}, \tag{77}$$

we may find the two governing equations for the problem from Eq. (41) and Eq. (72),

$$J = \frac{\sqrt{4\pi}\Gamma}{K\Omega} \frac{S_\infty(\theta_\mathrm{l})}{\sqrt{(1+\Omega\theta_\mathrm{l})\mathcal{Y}(\theta_\mathrm{l})}} \approx \frac{\sqrt{4\pi}\Gamma}{K\Omega} S_\infty(\theta_\mathrm{l}), \tag{78}$$

and

$$\theta_\mathrm{l} = 1 - HJ. \tag{79}$$

Note that the last approximation in Eq. (78) is applicable for the linearized (weak evaporation) models. For a given film thickness H, these two equations must in general be solved simultaneously in order to obtain J and θ_l. This includes using the function S_∞ from the chosen evaporation model, and having some representation of the saturation line in order to calculate the pressure-based driving force from a given liquid temperature.

However, if we use the highly simplified version of the evaporation models found in Sec. 2.8, we may arrive at a particularly simple and useful analytical form. By combining Eq. (55) and Eq. (63) we find that

$$S_\infty = \frac{r(\alpha)\phi(\theta_\mathrm{l})\Omega}{\sqrt{4\pi}\Gamma}\theta_\mathrm{l}. \tag{80}$$

We may then insert Eq. (80) into the rightmost form of Eq. (78) and assume that Γ is so small that $\phi \approx 1$ is reasonable. This yields a simple proportionality between the evaporation mass flux and the liquid superheat,

$$J = \frac{r(\alpha)}{K}\theta_\mathrm{l}. \tag{81}$$

When combined with Eq. (79), this gives a remarkably simple solution for the mass flux,

$$J = \frac{1}{H + \frac{K}{r(\alpha)}}. \tag{82}$$

and liquid superheat,

$$\theta_\mathrm{l} = \frac{1}{1 + H\frac{r(\alpha)}{K}}. \tag{83}$$

This is the kind of model found in previous works on thin-film flow such as Burelbach et al. (1988), Panzarella et al. (2000) and Aursand et al. (2018), due to its ease of coupling into a fluid mechanics context. Note that in this approximation, choice of specific evaporation model only affects the results through differences in the function $r(\alpha)$.

It is now worth noting the following points:

- The macroscopic driving force $\Omega \propto \Delta T_\mathrm{w}$ has little effect on the dimensionless evaporation rate J. This is because the scale j_0 is proportional to ΔT_w.
- Any deviation of $J(H)$ from Eq. (74) is by definition a non-equilibrium effect. From Eq. (82) it is then clear that K represents the relative strength of such effects, and that we approach the quasi-equilibrium approximation in the limit of $K \to 0$.
- For a given case and fluid, the value of K, and thus the non-equilibrium effects, may be increased by reducing the initial film thickness h_0.

3.3. Pressure driving-force

In the context of the liquid-film case, $\Delta\mathcal{Z}$ is an output from the calculation, not a given parameter like it was in Sec. 2. In general, after finding a solution to the system Eqs. (78) and (79), the driving force may be calculated from

$$\Delta\mathcal{Z} = \frac{p_\mathrm{s}(T_\mathrm{l}) - p_\infty}{p_\infty}, \qquad T_\mathrm{l} = T_\mathrm{s}\left(1 + \Omega\theta_\mathrm{l}\right). \tag{84}$$

Under the approximation of linearized saturation line, where Eq. (82) may be used, we find from Eq. (63) a very simple proportionality between driving force and liquid superheat,

$$\Delta\mathcal{Z} = \frac{\Omega}{\Gamma}\theta_\mathrm{l} = \frac{\Omega}{\Gamma}\left(\frac{1}{1 + H\frac{r(\alpha)}{K}}\right) \tag{85}$$

3.4. Thermodynamic state of the downstream vapor

The BEMM model also makes a prediction for the temperature discontinuity $\Delta T = T_\mathrm{l} - T_\infty$. While the temperature of the vapor does not couple back into the liquid-film evaporation problem here, it may be interesting to note the thermodynamic state of the vapor ejected from the liquid surface. The vapor temperature relative to the saturation temperature can be written as

$$\frac{T_\infty}{T_\mathrm{s}} = \left(1 + \Omega\theta_\mathrm{l}\right)\left(1 - \Delta\mathcal{Y}\right), \tag{86}$$

with a value above unity implying superheated vapor and a value below unity implying supersaturated vapor. The formulation shown in Eq. (86) nicely illustrates the two

contributing factors: The first factor $(1+\theta_\mathrm{l}\Omega)$ represents the liquid superheating, and the second factor $(1-\Delta\mathcal{Y})$ represents the temperature-decrease from liquid to vapor. The dimensionless vapor temperature may then be found from

$$\theta_\infty = \frac{1}{\Omega}\left(\frac{T_\infty}{T_\mathrm{s}} - 1\right). \tag{87}$$

For the simplified form of the BEMM model where also the saturation line is linearized, we may combine Eq. (53) with Eq. (63) in order to find $\Delta\mathcal{Y}$ as a function of θ_l, and then insert that into Eq. (86) and Eq. (87) to find

$$\theta_\infty = \left[1 - (1+\Omega\theta_\mathrm{l})\,\frac{r(\alpha)}{8\Gamma}\right]\theta_\mathrm{l}. \tag{88}$$

Once again we see that the vapor will be supersaturated if $r(\alpha) > 8\Gamma$. We also see that the degree of supersaturation will approximately be proportional to the degree of liquid superheat.

3.5. Time-evolution

If we assume that the liquid film remains uniform (i.e. without x-gradients) and define a dimensionless time $\tau = t/t_0$ with the evaporative time-scale

$$t_0 = \frac{h_0}{(j_0/\rho_\mathrm{l})} = \frac{\rho_\mathrm{l} h_0^2 L}{k_\mathrm{l}\Delta T_\mathrm{w}}, \tag{89}$$

the film-thickness $H(\tau)$ simply evolves according to

$$\frac{\partial H}{\partial \tau} = -J(H), \tag{90}$$

with the initial condition $H(0) = 1$. In general Eq. (90) must be integrated numerically. However, for the simplified model of Eq. (82) there is an analytical solution:

$$H(\tau) = \left[\left(\frac{K}{r}+1\right)^2 - 2\tau\right]^{1/2} - \frac{K}{r}. \tag{91}$$

This implies film dry-out at the time

$$\tau_\mathrm{dry} = \frac{1}{2} + \frac{K}{r}, \tag{92}$$

which shows clearly that non-equilibrium effects slow evaporation and delay dry-out. Note that even though the quasi-equilibrium limit ($K \to 0$) causes J to diverge at dry-out, it yields a well-defined answer for the dry-out time.

3.6. Summary of case parameters

We may summarize the case parameters as follows:

- **The relative wall superheat** (Ω): In order for the case to remain as illustrated in Fig. 6 it is necessary that $\Omega \ll 1$ to avoid heterogeneous nucleation at the solid surface.
- **The fluid's saturation line** (function $p_\mathrm{s}(T_\mathrm{l})$): For a given ambient pressure p_∞ this also determines the value of Γ, since according to the Clausius–Clapeyron relation Γ^{-1} is essentially the dimensionless slope of the saturation line $p_\mathrm{s}(T)$. Thus, the value of Γ may not be freely chosen if a specific saturation line is to be used. According to Trouton's rule we may expect $\Gamma \approx 0.1$.
- **The non-equilibrium factor**, (K): This number depends not only on fluid parameters, but also on the initial film thickness, $K \propto 1/h_0$. Thus, K may be used as a dimensionless measure of (inverse) film thickness. The value of K is usually quite negligible ($\approx 10^{-4}$) for liquid film thicknesses in the millimeter range, but grows to unity and beyond for submicrometer films.
- **Evaporation/condensation coefficient** (α): As seen from the approximation in Eq. (82), this mainly acts as a modifier on the non-equilibrium factor. For all the linearized models its effect is filtered through the function $r(\alpha)$, which depends on the specific evaporation model. By definition we must always have $\alpha \in [0,1]$, but how to choose a specific value is still the subject of much debate.

3.7. Demonstration: Evaporating water film

We will now demonstrate the use of kinetic theory evaporation models for the specific case of an evaporating water film in contact with water vapor at atmospheric pressure ($p_\infty = 101\,\mathrm{kPa}$). The case parameters are as follows:

- In order to have a somewhat strong evaporation while still staying below the nucleate boiling regime, we set the surface temperature so that $\Omega = 0.05$.
- The saturation line for water is represented by a smooth interpolation of real water-data from the NIST database (Linstrom and Mallard, 2017). Its slope at atmospheric pressure corresponds to $\Gamma \approx 0.074$.
- As discussed in Aursand et al. (2018, Sec. 2.2), we may reasonably choose $\alpha = 0.85$ for the evaporation/condensation coefficient.
- Since the dimensionless non-equilibrium factor (K) is dependent on film thickness scale h_0, its value is left as a variable. For water, non-equilibrium effects start becoming significant around $h_0 \approx 10\,\mu\mathrm{m}$ ($K \approx 0.01$), and rapidly grows in importance as the film becomes thinner.

We will mainly compare four evaporation models. The full nonlinear BEMM model requires numerically solving Eqs. (78) and (79) together with Eqs. (36) to (38). The linearized BEMM(L), HK and SM models require numerically solving Eqs. (78) and (79) together with Eq. (55).

Additionally, the combination of weak evaporation and linearized saturation line led to the direct approximate expression Eq. (82). For comparison this will also be computed for the three models BEMM(L), HK and SM.

We start by examining the initial evaporation rate of a liquid water film of some given initial thickness h_0. In other words, the solution at $H = 1$ is plotted for increasing K-values. Fig. 7 shows the evaporative driving-force $\Delta\mathcal{Z} = \Delta p_s/p_\infty$ resulting from the solutions. We see that even for extremely thin films ($K > 1$) the evaporative driving-force never grows very large. This means that we stay in the leftmost part of Fig. 3, where the linearizations are expected to work well.

The resulting interface temperatures are shown in Fig. 8. We see that the difference temperature jump grows large remarkably fast. For $K > 1$ the BEMM model shows that $\theta_l - \theta_\infty > 1$, which means that $T_l - T_\infty > \Delta T_w$. In other words, the temperature jump across the interface is larger than the wall superheat. Note that the downstream vapor, for this choice of α, is supersaturated for all nonzero values of K. Note also that while all the kinetic theory models give quite similar results for the liquid interface superheat, they are all in stark contrast to the quasi-equilibrium model, which by definition yields $\theta_l = \theta_\infty = 0$.

In Fig. 9 we see that the kinetic theory models, with the exception of the HK model, give very similar results for the evaporation mass flux. This includes the highly simplified forms given by Eq. (82). However, they are still very different from the predictions of the quasi-equilibrium approximation. Specifically, for $K > 1$ the quasi-equilibrium approximation overpredicts the mass flux by a factor of two and more.

In Fig. 10 we show the results of numerically integrating the ODE in Eq. (90) to zero thickness. For comparison, the simplified analytical solutions in Eq. (91) are also shown, including the quasi-equilibrium case ($K = 0$). We see that besides the HK model, all the kinetic theory models give approximately the same results. However, they predict a dry-out time that is 70% longer than what the quasi-equilibrium approximation implies.

4. Discussion

4.1. General considerations

It is clear from Fig. 3 that only the full nonlinear BEMM model is able to make reliably accurate predictions in the whole range of relevant evaporation rates. However, as seen both Figs. 3 and 5, the linearized BEMM(L) model is sufficient to predict the mass flux in the weak evaporation limit. Also, despite its theoretical inadequacies related to ignoring conservation of momentum and energy, the SM is also quite capable of predicting the mass flux. The HK model predicts only about half of this evaporation rate, and should not be used.

Even though the linearized BEMM(L) model has a significantly more complicated theoretical origin compared to the SM model, there is no reason to not use the former in the case of weak evaporation. The application of the two are identical, through the use of Eq. (61), besides some trivial differences in the functions $r(\alpha)$ and $\phi(T_l)$.

While the SM model is able to decently predict the evaporation rate, it is too simplistic to make an independent prediction for the downstream vapor temperature T_∞. This is another reason to use the BEMM(L) model. As seen in Fig. 4, the BEMM(L) model is a sufficient approximation to the full nonlinear model in the weak-evaporation regime.

With these points considered, it seems appropriate to recommend the BEMM model in general, including its linearized form if the driving force is weak ($\Delta\mathcal{Z} \ll 1$).

4.2. The liquid-film case

We may use the approximation in Eq. (85) to investigate whether or not the driving force $\Delta\mathcal{Z} = \Delta p_s/p_\infty$ is expected to be small. In the quasi-equilibrium limit ($K \to 0$), we get $\Delta\mathcal{Z} = 0$ as expected. By investigating the other extreme of $K \to \infty$, we see that the maximum attainable driving force is approximately $\Delta\mathcal{Z} = \Omega/\Gamma$. As discussed earlier, for liquid-film evaporation cases such as in Fig. 6, the wall superheat must be small/moderate ($\Omega \ll 1$). Since $\Gamma \approx 0.1$ for most fluids, this implies that the driving force will be in the region $\Delta\mathcal{Z} < 1$ regardless of K-value.

We see from Fig. 7 that $\Delta\mathcal{Z}$ remains especially small as long as the film thickness is large enough that $K < 1$. For the present test case this will only requires that the film thickness is over 100 nm. When this is the case, we are firmly placed in the weak-evaporation regime where BEMM(L) is an acceptable approximation of BEMM. On the other hand, using the HK or SM models would constitute a sacrifice of accuracy with no real gain in simplicity or utility compared to BEMM(L). Thus, we may once again recommend BEMM(L), unless the film is extremely thin. In fact, under the condition that $K < 1$, it appears that it is sufficient to use the further simplified version of BEMM(L) which uses a linearized saturation line. This means that one can directly apply Eq. (82) to find the mass flux J, Eq. (83) to find the liquid-side interface temperature θ_l, Eq. (88) to find the downstream vapor temperature θ_v, Eq. (91) to find the time-evolution of the film thickness $H(\tau)$.

While the linearized and simplified kinetic-theory based models appear to be sufficient for most of the reasonable range of K-values, it appears that K must be extremely small for the quasi-equilibrium approximation to be accurate. From Fig. 9 we see that the quasi-equilibrium approximation significantly overpredicts the evaporation mass flux for all values of K except the very small. The errors of the quasi-equilibrium approach may also have a qualitative impact on the model. A prominent example of this may be seen from the interface temperatures in Fig. 8. The quasi-equilibrium approximation specifies exactly $\theta_l = 0$ by definition, for all values of H. This

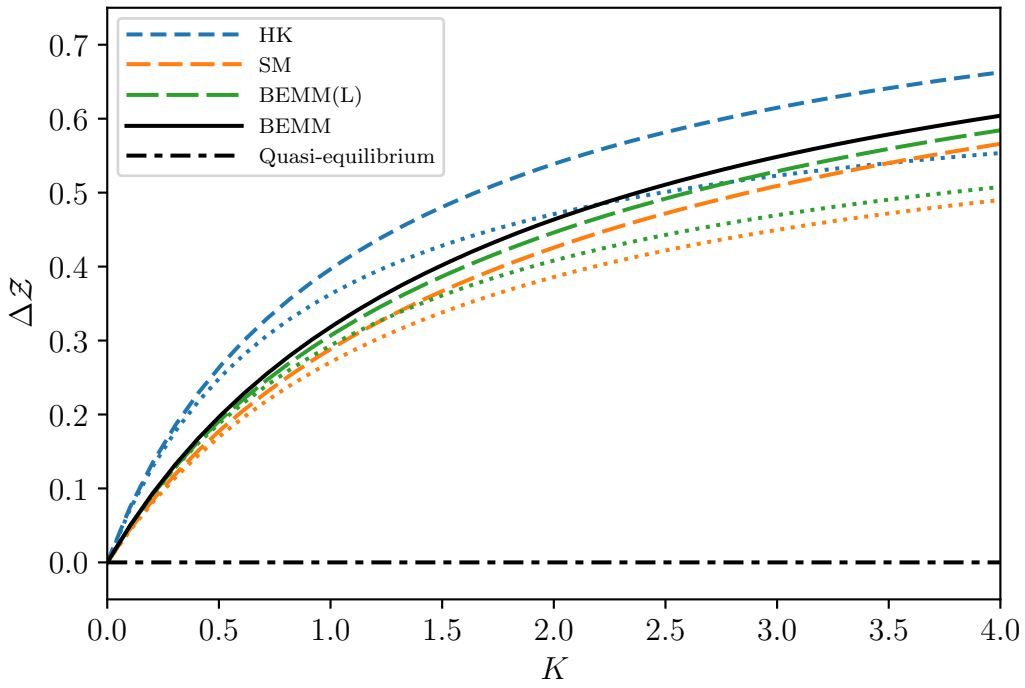

Figure 7: Initial evaporative driving force $\Delta\mathcal{Z} = \Delta p_\mathrm{s}/p_\infty$ as a function of film thickness in terms of $K \propto 1/h_0$. In addition to the four main models, the dotted curves show the results from the corresponding simplifications from Eq. (85).

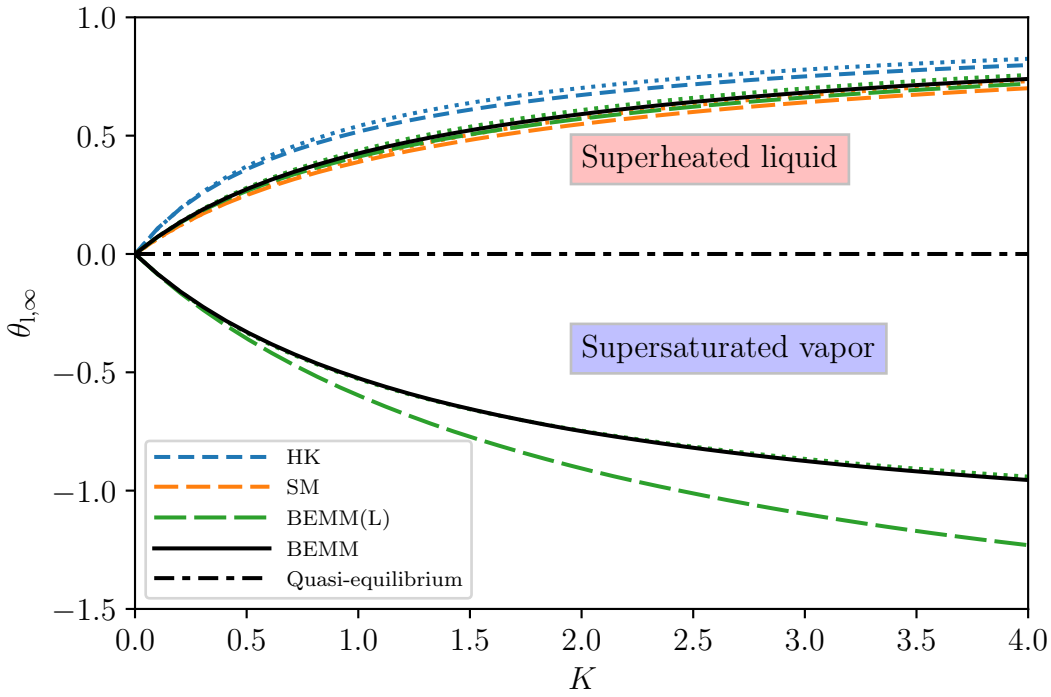

Figure 8: Initial liquid- and vapor-side temperature ($\theta = (T - T_\mathrm{s})/\Delta T_\mathrm{w}$) at the interface as a function of film thickness in terms of $K \propto 1/h_0$. In addition to the four main models, the dotted curves on the liquid side show the results of the corresponding simplifications from Eq. (83). Note how only the BEMM models make a prediction for the vapor state, and that in this case the simplified prediction by Eq. (88) (dotted line) is practically identical to the results of the full model.

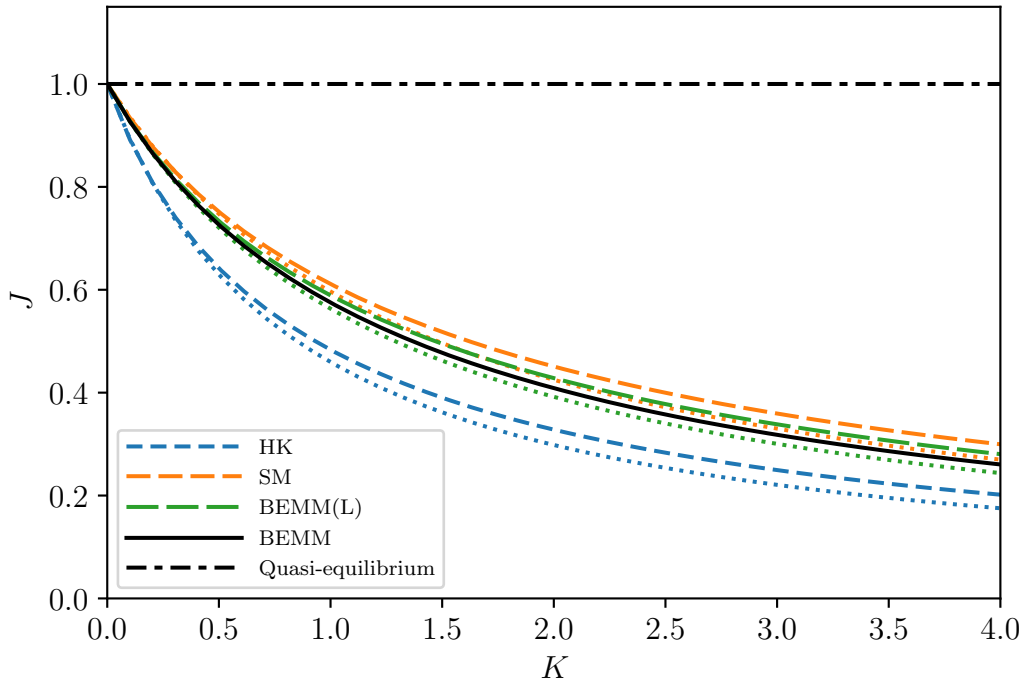

Figure 9: Initial evaporation mass flux as a function of film thickness in terms of $K \propto 1/h_0$. In addition to the four main models, the dotted curves show the results from the corresponding simplifications from Eq. (82).

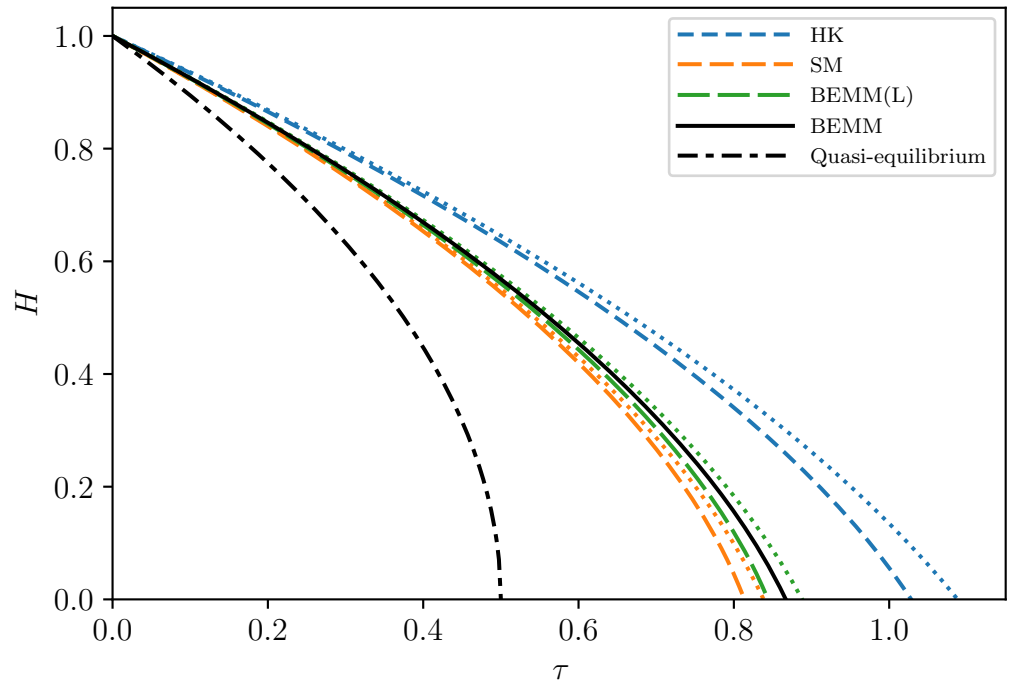

Figure 10: Film thickness plotted against dimensionless time (scaled by Eq. (89)), in a case where the initial film thickness is such that $K = 0.5$. In addition to the four main models, the dotted curves show corresponding simplified results from Eq. (91).

may have a significant qualitative effect, since it eliminates any thermocapillary effect at the evaporating interface (see Aursand et al. (2018)).

If one is interested only in the dry-out time, we see from Fig. 10 that every choice besides the HK or quasi-equilibrium model gives practically the same results. Even though the linearization behind BEMM(L) breaks down as H approaches zero, this does not matter for the end result because the relative time spent at these thicknesses is so small. Compared to the quasi-equilibrium approximation they predict a significantly longer time before dry-out. In Fig. 10 it is about 70% longer, but the specific number will depend on the value of K. Additionally, they show a qualitative difference in that the evaporation rate does not approach infinity as H approaches zero.

Finally, note that the recommendation of linearized evaporation models herein should not be taken as general for all cases of evaporation. They apply specifically for the liquid-film in Fig. 6 with moderate surface superheat.

5. Conclusions

We have concisely summarized the derivation of a handful of kinetic-theory evaporation models, and shown how they make predictions for the evaporation rate given a fundamental driving-force based on the liquid saturation pressure. We have also shown how these fundamental formulations found in the kinetic theory literature reduce to the highly simplified forms found in some fluid mechanics literature, Eq. (64). From studying these evaporation models we note the following:

- The liquid–vapor temperature-jump (ΔT) cannot be considered as an independent case parameter in addition to the pressure-based driving force (Δp_s). If the latter is specified, the temperature jump is a uniquely determined output.
- The older Hertz–Knudsen (HK) and Schrage–Mills (SM) models are unable to make an independent prediction for the temperature jump. In contrast, the Boltzmann Equation Moment Method (BEMM), both in its nonlinear and linearized form, is able to make such a prediction.
- As long as the evaporation is weak ($\Delta\mathcal{Z} \ll 1$), we recommend the linearized BEMM(L) model, Eq. (52). For very strong evaporation ($\Delta\mathcal{Z} > 1$) we must recommend its full nonlinear form.

We have also demonstrated how these evaporation models may be applied in a conventional evaporation problem, as an alternative to the commonly used quasi-equilibrium (QE) approximation. Based on the analysis of the liquid film evaporation case, we may conclude that:

- As shown in Fig. 9, the QE assumption should only be used if K is very small. For a fluid like water, this requires the film to be thicker than about 10 µm. For thinner films, the QE assumption will significantly overpredict the evaporation rate. Also, as seen in Fig. 8, the QE assumption completely ignores a very significant temperature jump across the interface. This may have an important qualitative impact even for thicker films.
- When non-equilibrium evaporation models are in fact necessary, is seems sufficient to use the BEMM(L) model with linearized saturation line. It gives both accurate evaporation rates and a prediction for the vapor temperature without much unneeded complexity. This means that the expressions in Eqs. (82), (83) and (88) may be used to find the evaporation rate, liquid-side interface temperature and vapor-side interface temperature, respectively.

In further work it would be interesting to examine the full implications of the non-equilibrium evaporation models for thin films. Assuming that the scale requirements mentioned in Sec. 3.1 are satisfied, these models could be included in stability analysis. As shown in Burelbach et al. (1988) and Aursand et al. (2018), the evaporation model affects many aspects of stability in both liquid and vapor thin-films, including vapor-thrust and thermocapillary effects. In particular, making the quasi-equilibrium approximation doesn't merely cause a quantitative error in the thermocapillary instabilities. In these evaporation cases, it completely eliminates the thermocapillary effect from the models.

Acknowledgements

This publication is based on results from the research project *Predicting the risk of rapid phase-transition events in LNG spills (Predict-RPT)*, performed under the MAROFF program. The authors acknowledge the Research Council of Norway (244076/O80) for support. Additional thanks to Bernhard Müller, Svend Tollak Munkejord, and Morten Hammer for discussions and feedback.

References

S.I. Anisimov. Evaporation of metal on absorbing laser radiation. *Journal of Experimental and Theoretical Physics*, 54(1):339–342, 1968.

K. Aoki and C. Cercignani. Evaporation and condensation on two parallel plates at finite reynolds numbers. *The Physics of Fluids*, 26(5):1163–1164, 1983. doi: 10.1063/1.864277.

K. Aoki, K. Nishino, Y. Sone, and H. Sugimoto. Numerical analysis of steady flows of a gas condensing on or evaporating from its plane condensed phase on the basis of kinetic theory: Effect of gas motion along the condensed phase. *Physics of Fluids A: Fluid Dynamics*, 3(9):2260–2275, 1991. doi: 10.1063/1.857907.

M. D. Arthur and C. Cercignani. Non-existence of a steady rarefied supersonic flow in a half-space. *Zeitschrift für angewandte Mathematik und Physik ZAMP*, 31(5):634–645, 1980. doi: 10.1007/BF01596163.

E. Aursand, S. H. Davis, and T. Ytrehus. Thermocapillary instability as a mechanism for film boiling collapse. *Journal of Fluid Mechanics*, 852:283–312, 2018. doi: 10.1017/jfm.2018.545.

J. P. Burelbach, S. G. Bankoff, and S. H. Davis. Nonlinear stability of evaporating/condensing liquid films. *Journal of Fluid Mechanics*, 195:463–494, 1988. doi: 10.1017/S0022112088002484.
V. P. Carey. *Liquid-vapor phase-change phenomena*. Hemisphere, New York, 1992. ISBN 1560320745.
C. Cercignani. Strong evaporation of a polyatomic gas. *Progress in Astronautics and Aeronautics*, 74:305–320, 1981.
C. Cercignani. *The Boltzmann Equation and Its Applications*. Springer, Berlin, 1988. ISBN 9781461210399.
J.W. Cipolla Jr, H. Lang, and S.K. Loyalka. Kinetic theory of evaporation and condensation. In K. Karamcheti, editor, *Rarefied Gas Dynamics*, pages 179–185. Academic Press, 1974. ISBN 978-0-12-398150-9. doi: 10.1016/B978-0-12-398150-9.50021-3.
R. V. Craster and O. K. Matar. Dynamics and stability of thin liquid films. *Reviews of modern physics*, 81(3):1131–1198, 2009. doi: 10.1103/RevModPhys.81.1131.
A. Frezzotti. A numerical investigation of the steady evaporation of a polyatomic gas. *European Journal of Mechanics-B/Fluids*, 26 (1):93–104, 2007. doi: 10.1016/j.euromechflu.2006.03.007.
A. Frezzotti and P. Barbante. Kinetic theory aspects of non-equilibrium liquid-vapor flows. *Mechanical Engineering Reviews*, 4(2):16–00540, 2017. doi: 10.1299/mer.16-00540.
H. Hertz. Ueber die verdunstung der flüssigkeiten, insbesondere des quecksilbers, im luftleeren raume. *Annalen der Physik*, 253(10): 177–193, 1882. doi: 10.1002/andp.18822531002.
M. Knudsen. Die maximale verdampfungsgeschwindigkeit des quecksilbers. *Annalen der Physik*, 352(13):697–708, 1915. doi: 10.1002/andp.19153521306.
M.N. Kogan. Kinetic theory in aerothermodynamics. *Progress in Aerospace Sciences*, 29(4):271–354, 1992. doi: 10.1016/0376-0421(92)90007-5.
M.N. Kogan and A.A. Abramov. Direct simulation solution of the strong evaporation and condensation problem. *Rarefied Gas Dynamics*, pages 1251–1257, 1991.
M.N. Kogan and N.K. Makashev. Role of the knudsen layer in the theory of heterogeneous reactions and in flows with surface reactions. *Fluid Dynamics*, 6(6):913–920, 1971. doi: 10.1007/BF01019794.
P. J. Linstrom and W. G. Mallard, editors. *NIST Chemistry WebBook, NIST Standard Reference Database Number 69*. National Institute of Standards and Technology, Gaithersburg MD, 20899, 2017. doi: 10.18434/T4D303. URL http://webbook.nist.gov.
R. Mager, G. Adomeit, and G. Wortberg. Theoretical and experimental investigation of the strong evaporation of solids. *Rarefied Gas Dynamics: Physical Phenomena*, 117:460–469, 1989.
A. F. Mills. *Heat and Mass Transfer*. CRC Press, Boca Raton, 1995. ISBN 9780256114430.
A. Oron, S. H. Davis, and S. G. Bankoff. Long-scale evolution of thin liquid films. *Reviews of modern physics*, 69(3):931–980, 1997. doi: 10.1103/RevModPhys.69.931.
C. H. Panzarella, S. H. Davis, and S. G. Bankoff. Nonlinear dynamics in horizontal film boiling. *Journal of Fluid Mechanics*, 402:163–194, 2000. doi: 10.1017/S0022112099006801.
Y.-P. Pao. Application of kinetic theory to the problem of evaporation and condensation. *The Physics of Fluids*, 14(2):306–312, 1971a. doi: 10.1063/1.1693429.
Y.-P. Pao. Temperature and density jumps in the kinetic theory of gases and vapors. *The Physics of Fluids*, 14(7):1340–1346, 1971b. doi: 10.1063/1.1693612.
A.J. Patton and G.S. Springer. A kinetic theory description of liquid vapor phase change. In *Proc. 6th International Symposium of Rarefied Gas Dynamics*, volume 2, pages 1497–1501, 1969.
A. H. Persad and C. A. Ward. Expressions for the evaporation and condensation coefficients in the hertz-knudsen relation. *Chemical reviews*, 116(14):7727–7767, 2016. doi: 10.1021/acs.chemrev.5b00511.
R. W. Schrage. *A theoretical study of interphase mass transfer*. Columbia University Press, New York, 1953.
P.N. Shankar and F. E. Marble. Kinetic theory of transient condensation and evaporation at a plane surface. *The physics of fluids*, 14(3):510–516, 1971. doi: 10.1063/1.1693464.
D. Sibold and H. M. Urbassek. Monte carlo study of knudsen layers in evaporation from elemental and binary media. *Physics of Fluids A: Fluid Dynamics*, 5(1):243–256, 1993. doi: 10.1063/1.858779.
Y. Sone and Y. Onishi. Kinetic theory of evaporation and condensation–hydrodynamic equation and slip boundary condition. *Journal of the Physical Society of Japan*, 44(6):1981–1994, 1978. doi: 10.1143/JPSJ.44.1981.
Y. Sone and H. Sugimoto. Kinetic theory analysis of steady evaporating flows from a spherical condensed phase into a vacuum. *Physics of Fluids A: Fluid Dynamics*, 5(6):1491–1511, 1993. doi: 10.1063/1.858587.
T. Ytrehus. One-dimensional effusive flow by the method of moments. In M Becker and M. Fiebig, editors, *Rarefied Gas Dynamics Vol I*. DFVLR-Press, Portz-Wahn, 1974.
T. Ytrehus. Theory and experiments on gas kinetics in evaporation. *Rarefied Gas Dynamics*, 2:1197–1212, 1977. doi: 10.2514/5.9781600865251.1197.1212.
T. Ytrehus. Molecular-flow effects in evaporation and condensation at interfaces. *Multiphase Science and Technology*, 9(3):205–327, 1997. doi: 10.1615/MultScienTechn.v9.i3.10.
T. Ytrehus and S. Østmo. Kinetic theory approach to interphase processes. *International journal of multiphase flow*, 22(1):133–155, 1996. doi: 10.1016/0301-9322(95)00056-9.

Appendix A. Kinetic theory details

The short-hand functions of S used in Sec. 2 are defined as follows:

$$\begin{aligned} F^{\pm}(S) &= \sqrt{\pi}S\left(\operatorname{erf}(S)\pm 1\right) + \mathrm{e}^{-S^2} \\ &= 1 \pm \sqrt{\pi}S + \mathcal{O}\left(S^2\right), \end{aligned} \tag{A.1}$$

$$\begin{aligned} G^{\pm}(S) &= \left(2S^2+1\right)\left(1\pm\operatorname{erf}(S)\right) \pm \frac{2}{\sqrt{\pi}}S\mathrm{e}^{-S^2} \\ &= 1 \pm \frac{4}{\sqrt{\pi}}S + \mathcal{O}\left(S^2\right), \end{aligned} \tag{A.2}$$

$$\begin{aligned} H^{\pm}(S) &= \frac{\sqrt{\pi}S}{2}\left(S^2+\frac{5}{2}\right)\left(\operatorname{erf}(S)\pm 1\right) + \frac{1}{2}(S^2+2)\mathrm{e}^{-S^2} \\ &= 1 \pm \frac{5\sqrt{\pi}}{4}S + \mathcal{O}\left(S^2\right). \end{aligned} \tag{A.3}$$